this problem, we attempted an inhibition analysis of HR-B peptides. Wild HVJ infectivity was significantly decreased by HR-B peptides, but no significant differences were observed in cholesterol-depleted HVJ with or without addition of cholesterol or HR-B peptides (Fig. 5g).

Discussion

In the present study, we demonstrated for the first time that cholesterol depletion from the plasma membrane of HVJ-infected cells increases subsequent HVJ production,

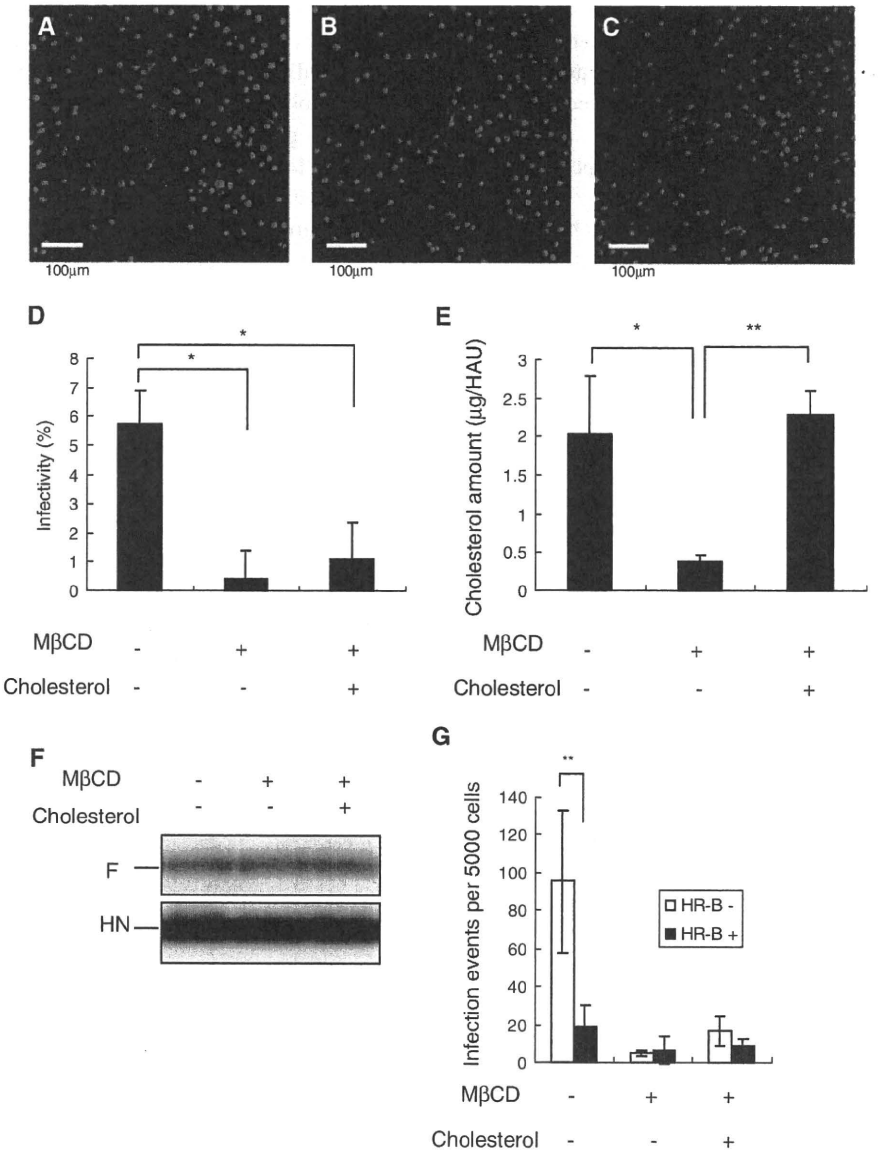

Fig. 5 Effects of envelope cholesterol depletion and restoration on HVJ infectivity. Infectivity of LLC-MK2 cells with control HVJ, directly cholesterol-depleted HVJ, and HVJ to which cholesterol was restored after methyl-beta cyclodextrin (MβCD) treatment was measured. (**a-c**) Each HVJ type was added to culture cells, and F protein expression on LLC-MK2 cells was visualized under 200-fold magnification by immunofluorescence microscopy. Blue dots are nuclei stained with DAPI, and red dots are F protein stained with Alexa 546. Immunofluorescence micrographs of LLC-MK2 cells infected with control HVJ (**a**), MβCD-treated HVJ (**b**), and (**c**) HVJ to which cholesterol was restored after MβCD treatment. (**d**) Infectivity of each HVJ type was determined by the ratio of F-protein-positive cells to all cells in a microscopic field. The data represent the mean ± standard deviation (n=5). A significant difference was obtained at $^*P < 0.01$, $^{**}P < 0.05$. (**e**) The amount of cholesterol in each HVJ type was measured by cholesterol oxidase and resorufin spectrophotometry. (**f**) Western blotting analysis of F and HN proteins of control HVJ, cholesterol-depleted HVJ, and HVJ to which cholesterol was restored after cholesterol depletion. (**g**) HVJ, cholesterol-depleted HVJ, and HVJ to which cholesterol was restored after depletion were applied to LLC-MK2 cells with or without HA-HR-B peptide. Infected cells were detected by immunostaining of the F protein. Stained cells were counted using the ImageJ program. A significant difference was obtained at $^*P < 0.05$

presumably by accelerating the process of budding of viral particles.

A previous study of the effect of cellular cholesterol depletion on HVJ production showed that cellular cholesterol depletion does not increase HVJ production but results in a corresponding increase in the M protein composition following MβCD treatment [7]. Here, we attempted to determine the effect of various MβCD treatment conditions on cellular cholesterol depletion and cell viability. Under the conditions of a 6-h incubation of cells with 1% MβCD, we succeeded in approximately 90% depletion of cellular cholesterol without affecting cell viability. Our conditions were more drastic than those used in the previous study described above, which caused approximately 60% depletion of cellular cholesterol [7]. Under our optimized conditions of MβCD treatment, HVJ production from LLC-MK2 cells was significantly increased. We also found that the HVJ that was produced had different properties. By sucrose gradient analysis, we first isolated HVJ that had different densities and diameters. In addition, the HN protein level of HVJ-CD was greater than that of F protein, unlike in wild-type HVJ (Fig. 4a, b). HVJ-CD infectivity was lower than that of wild-type HVJ. Although the previous study [7] also reported that the infectivity of HVJ-CD was lowered overall, we further examined the infectivity of each fraction of HVJ-CD separated by sucrose gradient centrifugation and demonstrated that none of the fractions showed significant infectivity. These results resemble those obtained in cholesterol depletion experiments with Newcastle disease virus (NDV) [16]. Lee et al [18]. also showed that infectious Japanese encephalitis virus and dengue virus serotype 2 production are decreased markedly in cells treated with MβCD.

Cholesterol in the cellular membrane is well known to influence the lipid fluidity of the cell membrane [5]. A higher content of cholesterol in liposomes is also known to make their membranes more rigid, resulting in a reduction in lipid fluidity [31]. Because M protein functions to assemble HN and F proteins at the HVJ budding site of the cell membrane, cholesterol depletion from the cell membrane may affect M-protein-mediated assembly of HN and F proteins when cell membrane fluidity is increased. Our results also support this hypothesis by showing an increase in M-protein-mediated VLP production from MβCD-treated cells. Previous studies have demonstrated the influence of cholesterol-rich microdomain disruption by MβCD. In a study with HIV, cells were treated with MβCD, and the release of virion-associated p24 was reduced by 70-80% [27]. However, in a study with influenza virus, lipid raft disruption by MβCD-mediated cholesterol depletion of virus-infected cells increased the release of virus particles and adversely affected virus infectivity [3]. The previous NDV study indicated that when cells were treated with MβCD, the amount of virion-derived NP released increased but the amount of M and F did not change, and HN was reduced, which suggested that particles released from cholesterol-extracted cells may be structurally abnormal [16]. The previous study of HVJ mentioned above also showed that M protein suppression did not provoke an alteration in the cholesterol-rich microdomain composition, although under these conditions, assembly leading to budding was significantly perturbed, as seen by a significant decrease in virus particle production. Taken together, these observations strongly suggest that the cholesterol-rich microdomain fractions do not constitute sites of viral component assembly directly related to virus particle production [7].

The reason why the infectivity of HVJ-CD was markedly impaired compared to that of wild-type HVJ is currently unknown. The data shown in Fig. 4b and e suggest that HVJ-CD envelope proteins in fractions 3-12 were presumably present on the viral envelope. However, we could not identify both F and HN proteins on any particle. Therefore, the first possibility is that cholesterol depletion of host cells reflects increased release of multiple vesicle populations, each harboring only a subset of the viral proteins. The second possibility is that HVJ-CD may lose the optimal HN/F protein composition required for sufficient infectivity [24], even though each particle retains both F and HN proteins. Because the amounts of intracellular F and HN proteins did not differ between the control and cholesterol-depleted LLC-MK2 cells, membrane cholesterol may directly affect the HN/F protein composition at the time of HVJ budding from the cellular membrane. A third possibility is that the cholesterol composition in the viral envelope may directly affect infectivity. To examine these possibilities, we directly treated HVJ with MβCD and found that the infectivity of wild-type HVJ was markedly disrupted by MβCD treatment (Fig. 5a-d). Because the amount of each protein was not altered before or after MβCD treatment (Fig. 5f), envelope cholesterol depletion appears to directly affect HVJ infectivity without altering the HN/F protein ratio. These results may exclude the first and the second possibility raised above and support the third possibility. This suggests that a significant reduction in envelope cholesterol in HVJ-CD has a more direct effect on such impaired infectivity. However, replenishment of cholesterol in the MβCD-treated HVJ, which returned the membrane cholesterol level to that of untreated HVJ, did not recover the lost infectivity (Fig. 5d, e). Our results demonstrate that cholesterol depletion causes an irreversible change in the function of the HVJ F protein on the envelope, which is not fully recoverable after cholesterol reconditioning. These results suggest that reconstruction of cholesterol and viral proteins on the viral envelope may be

necessary for the infectivity of HVJ. Thus, membrane cholesterol may play an essential role in controlling the HN and F protein properties in the budding process on the cell membrane and in maintaining the infectivity of HVJ. This conclusion is also supported by the HR-B peptide experiments; however, we cannot exclude the possibility that the low level of infection by cholesterol-depleted particles represents experimental background rather than "specific" infection. Nevertheless, the mechanism of cholesterol-dependent infectivity may not be commonly applied to other viruses, such as NDV, since cholesterol depletion does not affect the infectivity of NDV [16].

MβCD is well known to deplete mainly membrane cholesterol, although MβCD has also been shown to partially reduce phospholipids in the cell membrane [26]. Since HVJ also contains phospholipids in its envelope, a decrease in phospholipids by MβCD may also have affected infectivity. Further investigation to elucidate the precise role of these lipids on the infectivity of HVJ and other viruses may provide new perspectives for developing novel strategies to treat virus infections.

References

1. Ali A, Nayak DP (2000) Assembly of Sendai virus: M protein interacts with F and HN proteins and with the cytoplasmic tail and transmembrane domain of F protein. Virology 276:289–303
2. Atger VM, de la Llera Moya M, Stoudt GW, Rodrigueza WV, Phillips MC, Rothblat GH (1997) Cyclodextrins as catalysts for the removal of cholesterol from macrophage foam cells. J Clin Invest 99:773–780
3. Barman S, Nayak DP (2007) Lipid raft disruption by cholesterol depletion enhances influenza A virus budding from MDCK cells. J Virol 81:12169–12178
4. Chazal N, Gerlier D (2003) Virus entry, assembly, budding, and membrane rafts. Microbiol Mol Biol Rev 67:226–237 (table of contents)
5. Davis PJ, Poznansky MJ (1987) Modulation of 3-hydroxy-3-methylglutaryl-CoA reductase by changes in microsomal cholesterol content or phospholipid composition. Proc Natl Acad Sci USA 84:118–121
6. Garcin D, Pelet T, Calain P, Roux L, Curran J, Kolakofsky D (1995) A highly recombinogenic system for the recovery of infectious Sendai paramyxovirus from cDNA: generation of a novel copy-back nondefective interfering virus. EMBO J 14:6087–6094
7. Gosselin-Grenet AS, Mottet-Osman G, Roux L (2006) From assembly to virus particle budding: pertinence of the detergent resistant membranes. Virology 344:296–303
8. Harder T, Simons K (1997) Caveolae, DIGs, and the dynamics of sphingolipid-cholesterol microdomains. Curr Opin Cell Biol 9:534–542
9. Hasan MK, Kato A, Muranaka M, Yamaguchi R, Sakai Y, Hatano I, Tashiro M, Nagai Y (2000) Versatility of the accessory C proteins of Sendai virus: contribution to virus assembly as an additional role. J Virol 74:5619–5628
10. Hosaka Y, Shimizu YK (1972) Artificial assembly of envelope particles of HVJ (Sendai virus). I. Assembly of hemolytic and fusion factors from envelopes solubilized by Nonidet P40. Virology 49:627–639
11. Ilangumaran S, Hoessli DC (1998) Effects of cholesterol depletion by cyclodextrin on the sphingolipid microdomains of the plasma membrane. Biochem J 335(Pt 2):433–440
12. Kaneda Y, Nakajima T, Nishikawa T, Yamamoto S, Ikegami H, Suzuki N, Nakamura H, Morishita R, Kotani H (2002) Hemagglutinating virus of Japan (HVJ) envelope vector as a versatile gene delivery system. Mol Ther 6:219–226
13. Kawachi M, Tamai K, Saga K, Yamazaki T, Fujita H, Shimbo T, Kikuchi Y, Nimura K, Nishifuji K, Amagai M, Uitto J, Kaneda Y (2007) Development of tissue-targeting hemagglutinating virus of japan envelope vector for successful delivery of therapeutic gene to mouse skin. Hum Gene Ther 18:881–894
14. Kilsdonk EP, Yancey PG, Stoudt GW, Bangerter FW, Johnson WJ, Phillips MC, Rothblat GH (1995) Cellular cholesterol efflux mediated by cyclodextrins. J Biol Chem 270:17250–17256
15. Klein U, Gimpl G, Fahrenholz F (1995) Alteration of the myometrial plasma membrane cholesterol content with beta-cyclodextrin modulates the binding affinity of the oxytocin receptor. Biochemistry 34:13784–13793
16. Laliberte JP, McGinnes LW, Peeples ME, Morrison TG (2006) Integrity of membrane lipid rafts is necessary for the ordered assembly and release of infectious Newcastle disease virus particles. J Virol 80:10652–10662
17. Lamb RA, Kolakofsky D (1996) Paramyxoviridae : the viruses and their replication. In: "Fields Virol", 3rd edn. Raven Press, New York, pp 1177–1204
18. Lee CJ, Lin HR, Liao CL, Lin YL (2008) Cholesterol effectively blocks entry of flavivirus. J Virol 82:6470–6480
19. Li HO, Zhu YF, Asakawa M, Kuma H, Hirata T, Ueda Y, Lee YS, Fukumura M, Iida A, Kato A, Nagai Y, Hasegawa M (2000) A cytoplasmic RNA vector derived from nontransmissible Sendai virus with efficient gene transfer and expression. J Virol 74:6564–6569
20. Lin S, Naim HY, Rodriguez AC, Roth MG (1998) Mutations in the middle of the transmembrane domain reverse the polarity of transport of the influenza virus hemagglutinin in MDCK epithelial cells. J Cell Biol 142:51–57
21. Lu YE, Kielian M (2000) Semliki forest virus budding: assay, mechanisms, and cholesterol requirement. J Virol 74:7708–7719
22. Manie SN, Debreyne S, Vincent S, Gerlier D (2000) Measles virus structural components are enriched into lipid raft microdomains: a potential cellular location for virus assembly. J Virol 74:305–311
23. Maziere JC, Landureau JC, Giral P, Auclair M, Fall L, Lachgar A, Achour A, Zagury D (1994) Lovastatin inhibits HIV-1 expression in H9 human T lymphocytes cultured in cholesterol-poor medium. Biomed Pharmacother 48:63–67
24. Nakanishi M, Uchida T, Kim J, Okada Y (1982) Glycoproteins of Sendai virus (HVJ) have a critical ratio for fusion between virus envelopes and cell membranes. Exp Cell Res 142:95–101
25. Neufeld EB, Cooney AM, Pitha J, Dawidowicz EA, Dwyer NK, Pentchev PG, Blanchette-Mackie EJ (1996) Intracellular trafficking of cholesterol monitored with a cyclodextrin. J Biol Chem 271:21604–21613
26. Ohtani Y, Irie T, Uekama K, Fukunaga K, Pitha J (1989) Differential effects of alpha-, beta- and gamma-cyclodextrins on human erythrocytes. Eur J Biochem 186:17–22
27. Ono A, Freed EO (2001) Plasma membrane rafts play a critical role in HIV-1 assembly and release. Proc Natl Acad Sci USA 98:13925–13930
28. Ono A, Waheed AA, Freed EO (2007) Depletion of cellular cholesterol inhibits membrane binding and higher-order multimerization of human immunodeficiency virus type 1 Gag. Virology 360:27–35

29. Pickl WF, Pimentel-Muinos FX, Seed B (2001) Lipid rafts and pseudotyping. J Virol 75:7175–7183
30. Russell CJ, Jardetzky TS, Lamb RA (2001) Membrane fusion machines of paramyxoviruses: capture of intermediates of fusion. EMBO J 20:4024–4034
31. Saeki Y, Matsumoto N, Nakano Y, Mori M, Awai K, Kaneda Y (1997) Development and characterization of cationic liposomes conjugated with HVJ (Sendai virus): reciprocal effect of cationic lipid for in vitro and in vivo gene transfer. Hum Gene Ther 8:2133–2141
32. Scheiffele P, Roth MG, Simons K (1997) Interaction of influenza virus haemagglutinin with sphingolipid-cholesterol membrane domains via its transmembrane domain. EMBO J 16:5501–5508
33. Sugahara F, Uchiyama T, Watanabe H, Shimazu Y, Kuwayama M, Fujii Y, Kiyotani K, Adachi A, Kohno N, Yoshida T, Sakaguchi T (2004) Paramyxovirus Sendai virus-like particle formation by expression of multiple viral proteins and acceleration of its release by C protein. Virology 325:1–10
34. Takimoto T, Murti KG, Bousse T, Scroggs RA, Portner A (2001) Role of matrix and fusion proteins in budding of Sendai virus. J Virol 75:11384–11391
35. Tozawa H, Komatsu H, Ohkata K, Nakajima T, Watanabe M, Tanaka Y, Arifuku M (1986) Neutralizing activity of the antibodies against two kinds of envelope glycoproteins of Sendai virus. Arch Virol 91:145–161
36. Watanabe K, Okada Y (1974) A new method for propagation of HVJ (Sendai virus) in vitro: high sensitivity and productivity in spreading cultures of fragmented chorioallantoic membrane of chick embryos. Biken J 17:51–58
37. Yura Y, Matsumoto R, Sumi T, Kusaka J (2003) Effect of Ca2+-dependent cell death on the release of herpes simplex virus. Arch Virol 148:221–235
38. Zhang J, Pekosz A, Lamb RA (2000) Influenza virus assembly and lipid raft microdomains: a role for the cytoplasmic tails of the spike glycoproteins. J Virol 74:4634–4644

Accepted Date : 27-Feb-2011

Article type : Item of Correspondence

24 January, 2011

Correspondence

Vörner type palmoplantar keratoderma: novel *KRT9* mutation associated with knuckle pad-like lesion and recurrent mutation causing digital mutilation

N. Umegaki, H. Nakano,* K. Tamai,** Y. Mitsuhashi,*** E Akasaka,* D. Sawamura* and I. Katayama

Department of Dermatology, Osaka University Graduate School of Medicine
*Department of Dermatology, Hirosaki University Graduate School of Medicine
** Department of Stem Cell Therapy Science, Osaka University Graduate School of Medicine
*** Department of Dermatology, Tokyo Medical University

Key words: palmoplantar keratoderma, Vörner type, Keratin 9, digital mutilation, pseudoainhum

The authors declare no conflict of interest.

Address for correspondence:
Hajime Nakano, M.D.
Department of Dermatology, Hirosaki University Graduate School of Medicine,
5 Zaifu-cho, Hirosaki 036-8562, Japan
TEL: +81-172-39-5087
FAX: +81-172-37-6060
E-mail: hnakano@cc.hirosaki-u.ac.jp

MADAM, Epidermolytic palmoplantar keratoderma, Vörner type (EPPK, OMIM 144200) is an autosomal dominantly inherited skin disease caused by mutations in the keratin 9 gene (*KRT9*) and rarely in the keratin 1 gene. This condition is characterized by diffuse yellow thickening of the skin of the palms and soles, sharply offset by erythematous margins. Histopathologically, EPPK presents the characteristic features of epidermolytic hyperkeratosis. This report concerns two Japanese EPPK families associated with characteristic cutaneous manifestations: knuckle pad-like lesions associated with a novel nonsense *KRT9* mutation and digital mutilation caused by a recurrent *KRT9* mutation.

The proband of Family 1 was a 12-year-old Japanese girl presenting with hyperkeratosis of palms and soles since soon after birth (Figure 1a). Hypertrophic plaques with erythema were noted on the dorsal aspects of the distal phalanges of the hands (Figure 1a, lower panel). Similar lesions, but to a lesser extent, were seen on the toes (not shown). No other family members were affected. Histopathology showed epidermolytic hyperkeratosis with large irregular keratohyaline granules and vacuolization of keratinocytes in the upper spinous and granular layers (not shown).

The proband of Family 2 was a 58-year-old Japanese woman presenting with hyperkeratosis of palms and soles developed soon after birth. Her father and elder sister had similar hyperkeratotic skin changes. In the second decade of her life, the proband first noted that the fifth toes felt mildly constricted. Since then, the constriction gradually progressed with accompanying numbness of the fifth toes. When she was 50 years old, the constricted fifth toes became detached spontaneously and one by one with no traumatic etiology (Figure 1b, arrows). Slight constriction of the finger joints of the proband was observed, especially of the middle interphalangeal joints (Figure 1b, arrowheads). The other affected individuals did not show any constrictive changes in their fingers or toes nor any knuckle pad-like lesions. Histopathology indicated epidermolytic hyperkeratosis with vacuolization of the granular layers (not shown).

The genomic DNA samples extracted from the probands and their family members were subjected to mutation analyses. In the probands, all the *KRT9* exons and their flanking exon/intron junctions were amplified by PCR and the PCR products were directly sequenced. Mutational analysis

revealed a C-to-T transition at the nucleotide position 1282 (c.1282C>T) in exon 6 of *KRT9* in the proband of Family 1 (Fig. 2a), but not in the healthy parents, suggesting that this nucleotide change is a *de novo* mutation. This nucleotide substitution is expected to transform the corresponding amino acid glutamine into a stop codon (p.Q428X) within the 2B rod domain of the keratin 9 protein. Restriction fragment length polymorphism analyses (RFLP) using the restriction enzyme *Bsa*WI demonstrated that this nucleotide change was not present in 102 controls. In the proband of Family 2, direct sequencing demonstrated a C-to-T transition at nucleotide position 487 (c.487C>T). The proband's elder sister, also affected by EPPK, had the same mutation (not shown). This nucleotide substitution is thought to transform the corresponding amino acid arginine into tryptophan (p.R163W) within the 1A rod domain of the keratin 9 protein (Figure 2b).

To date, six EPPK families associated with knuckle pad-like lesions have been confirmed to have *KRT9* mutations.[1-6] All these mutations are missense mutations and reside in the 1A rod domain, while the mutation identified in Family 1 reported here is a nonsense mutation, resulting in deletion of one-third of the 2B rod domain in addition to the tail domain. To

the best of our knowledge, no nonsense *KRT9* mutation has been reported in cases with EPPK. In Family 2, we identified the R163W mutation in exon 1 of *KRT9*. It is well known that position 163 of the keratin 9 protein represents a mutational "hot spot", since this amino acid position has been reported as mutated in 32 out of 78 cases with EPPK (Human Intermediate Filament Database, www.interfil.org). In the previous cases with EPPK, however, no digital mutilation has been reported. It should be noted that a Japanese EPPK case with slight constriction of the fifth toes has been recently reported and the proband of that study had the same mutation as that of our case.[7] The distinct phenotypical heterogeneity in Family 2 may be explained by additional genetic and/or epigenetic factors in the proband. Pseudoainhum can be seen in other palmoplantar keratodermas (PPK) such as Vohwinkel syndrome, Olmsted syndrome and Papillon-Lefèvre syndrome, as well as in non-PPK states including psoriasis, morphea and erythropoietic protoporphyria.[8] Although the pathogenetic mechanism of pseudoainhum has not yet been elucidated, therapeutic intervention using oral acitretin reportedly provides relief for constriction of the fingers.[8] Therefore, monitoring early signs of digital constriction and performing prompt

therapeutic intervention may be necessary for preventing digital mutilation in PPK patients.

References

1 Lu Y, Guo C, Liu Q *et al.* A novel mutation of keratin 9 in epidermolytic palmoplantar keratoderma combined with knuckle pads. *Am J Med Genet A* 2003; **120A**: 345-9.

2 Küster W, Reis A, Hennies HC. Epidermolytic palmoplantar keratoderma of Vörner: re-evaluation of Vörner's original family and identification of a novel keratin 9 mutation. *Arch Dermatol Res* 2002; **294**: 268-72.

3 Hamada T, Ishii N, Karashima T *et al.* The common *KRT9* gene mutation in a Japanese patient with epidermolytic palmoplantar keratoderma and knuckle pad-like keratoses. *J Dermatol* 2005; **32**: 500-2.

4 Chiu HC, Jee SH, Sheen YS *et al.* Mutation of keratin 9 (R163W) in a family with epidermolytic palmoplantar keratoderma and knuckle pads. *J Dermatol Sci.* 2007; **45**: 63-5

5 Li M, Yang LJ, Hua HK *et al.* Keratin-9 gene mutation in epidermolytic palmoplantar keratoderma combined with knuckle pads in a large Chinese family. *Clin Exp Dermatol* 2009; **34**: 26-8.

6 Codispoti A, Colombo E, Zocchi L *et al.* Knuckle pads, in an epidermal palmoplantar keratoderma patient with Keratin 9 R163W transgrediens expression. *Eur J Dermatol* 2009; **19**: 114-8.

7 Funakushi N, Mayuzumi N, Sugimura R *et al.* Epidermolytic palmoplantar keratoderma with constriction bands on bilateral fifth toes. *Arch Dermatol* 2009: **145**: 609-10

8 Mashhood AA, Humayun A, Saleem M *et al.* Papillon-Lefèvre syndrome associated with pseudoainhum. *J Am Acad Dermatol* 2004; **51**: S134-5.

Figure legends

Figure 1. (a) Hyperkeratosis of palms of the proband of Family 1. Knuckle pad-like lesions were noted on the dorsal aspects of the distal phalangeal joints and to a lesser extent, on the middle interphalangeal joints. (b) Hyperkeratosis of palms and soles of the proband of Family 2. Mutilation of bilateral fifth toes (arrow).

Figure 2. Direct sequence analyses. (a) In the proband of Family 1, a heterozygous nonsense mutation c.1282C>T (p.Q428X) was identified (upper panel). Lower panel; sequence of the father. (b) In the proband of Family 2, a heterozygous missense mutation c.487C>T (p.R163W) was detected (upper panel). Lower panel; sequence of the asymptomatic sister.

Figure 1a

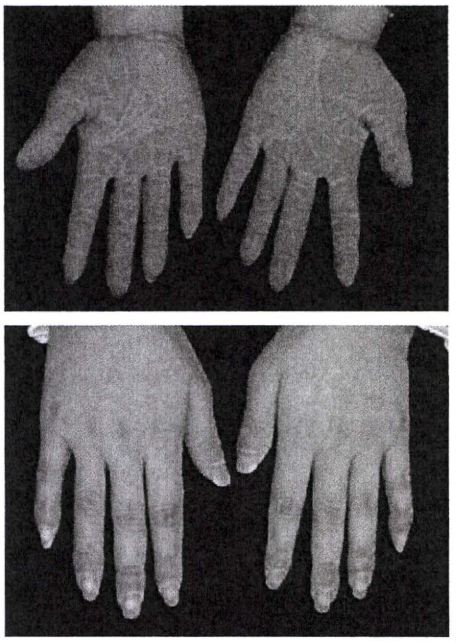

Figure 1b

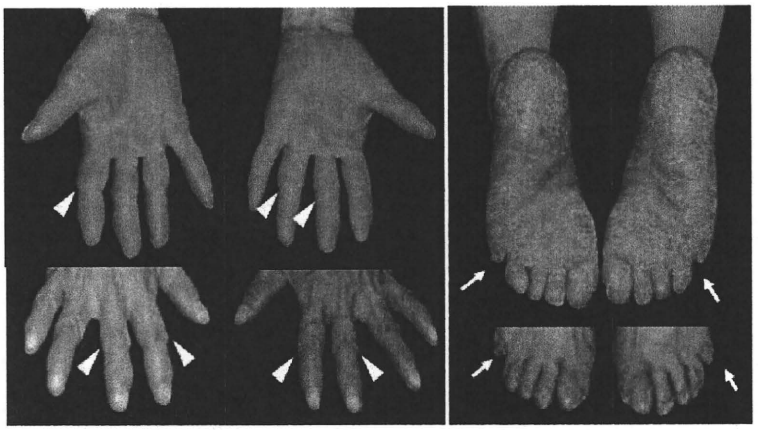

Figure 2

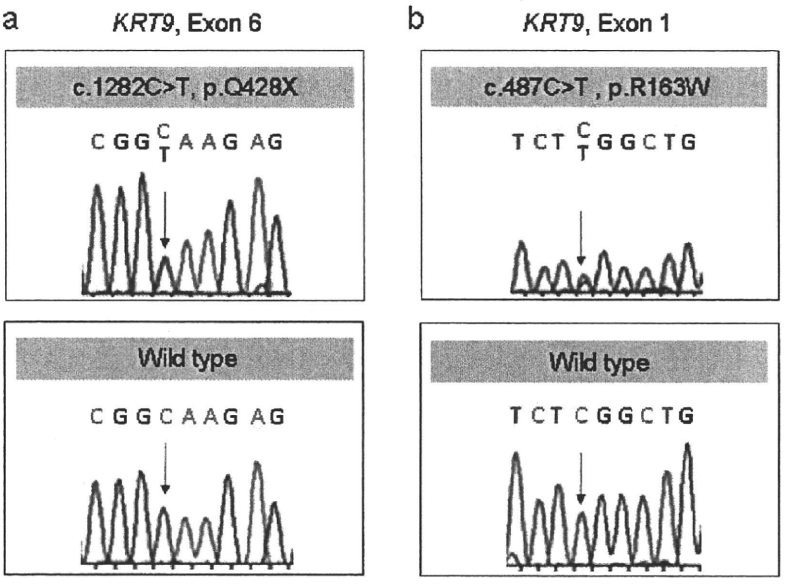
a
KRT9, Exon 6
c.1282C>T, p.Q428X
CGG C/T AAG AG
Wild type
CGGCAAG AG
b
KRT9, Exon 1
c.487C>T , p.R163W
TCT C/T GGCTG
Wild type
TCT CGGCTG

G Model
LR-4150; No. of Pages 7
ARTICLE IN PRESS

Leukemia Research xxx (2011) xxx–xxx

Contents lists available at ScienceDirect

Leukemia Research

journal homepage: www.elsevier.com/locate/leukres

Predictability of the response to tyrosine kinase inhibitors via *in vitro* analysis of Bcr-Abl phosphorylation

Masaru Shibata[a], Sachiko Ezoe[a,*], Kenji Oritani[a], Keiko Matsui[a], Masahiro Tokunaga[a], Natsuko Fujita[a], Yuri Saito[a], Takayuki Takahashi[b], Masayuki Hino[c], Itaru Matsumura[d], Yuzuru Kanakura[a]

[a] *Hematology and Oncology, Osaka University, Graduate School of Medicine, 2-2 Yamada-oka, Suita, Osaka 565-0871, Japan*
[b] *Kobe City Medical Center General Hospital, Kobe, Japan*
[c] *Department of Hematology, Graduate School of Medicine, Osaka City University, Osaka, Japan*
[d] *Department of Internal Medicine, Kinki University School of Medicine, Sayama, Japan*

ARTICLE INFO

Article history:
Received 16 December 2010
Received in revised form 12 January 2011
Accepted 14 January 2011
Available online xxx

Keywords:
CML
Tyrosine kinase inhibitor
Bcr-Abl
Crkl
Phosphorylation
Immunoblot

ABSTRACT

It would be of great value to predict the efficacy of tyrosine kinase inhibitors (TKIs) in the treatment of individual CML patients. We propose an immunoblot system for detecting the phosphorylation of Crkl, a major target of Bcr-Abl, in blood samples after *in vitro* incubation with TKIs. When the remaining phosphorylated Crkl after treatment with imatinib was evaluated as the "residual index (RI)", high values were found in accordance with imatinib resistance. Moreover, RI reflected the outcome of imatinib- as well as second generation TKIs with a high sensitivity and specificity. Therefore, this system should be useful in the selection of TKIs.

1. Introduction

The introduction of tyrosine kinase inhibitors (TKIs) targeting Bcr-Abl have dramatically improved the treatment of CML. Imatinib mesylate (Gleevec; Novartis Pharmaceuticals, East Hanover, NJ) was shown to induce high rates of cytogenetic and molecular responses, resulting in greatly prolonged survival in CML patients [1,2]. However, despite the remarkable improvement in survival and responsiveness with imatinib-treatment, a considerable proportion of the patients treated with imatinib have been reported to exhibit either primary or secondary resistance or intolerance [3–5]. Clinical resistance to imatinib can result from mutations in the Abl kinase domain at residues that directly contact imatinib or that influence imatinib binding [6]. As resistance can also arise in the absence of Bcr-Abl mutations, other mechanisms of resistance and disease progression may exist, including Bcr-Abl-independent signaling in CML cells [7]. To overcome the resistance and intolerance to imatinib, efforts have been made to develop second- and third-generation TKIs. Examples of such inhibitors include nilotinib (Tasigna, Novartis) [8], dasatinib (Sprycel, Bristol-Myers Squibb) [9] and other TKIs under clinical investigation such as bosutinib [10] and INNO-406 [11]. These TKIs are significantly more potent than imatinib and have exhibited efficacy against many types of imatinib-resistant Bcr-Abl mutants. Furthermore, they are also candidates for first-line therapy, as there is a need to improve the results achieved with imatinib [12–14]. In parallel with the entrance of new therapeutic compounds, an important question is which TKI is the most appropriate to each CML patient.

To establish a system with which we can predict the response of each patient to TKIs, we investigated in this study the phosphorylation of Crkl, a major target of Bcr-Abl, after *in vitro* incubation with or without TKIs in peripheral blood (PB) samples from patients either newly diagnosed or resistant to imatinib. It is demonstrated that this *in vitro* analysis system is highly reflective of the clinical response to TKIs of CML patients, and these data should prove useful in selecting TKIs in individual cases.

2. Patients, materials and methods

2.1. Patient blood samples

Thirty-one patients with CML in the chronic phase (CP) were included in this study (Table 1). The optimal response, response and resistance were defined in accordance with the European Leukemia Net (ELN) recommendations [15,16]. Briefly, an "optimal response" to imatinib means achieving a complete hematological response (CHR) at 3 months or complete cytogenetic response (CCyR) at

* Corresponding author. Tel.: +81 6 6879 3871; fax: +81 6 6879 3879.
E-mail address: sezoe@bldon.med.osaka-u.ac.jp (S. Ezoe).

0145-2126/$ – see front matter © 2011 Elsevier Ltd. All rights reserved.
doi:10.1016/j.leukres.2011.01.012

Please cite this article in press as: Shibata M, et al. Predictability of the response to tyrosine kinase inhibitors via *in vitro* analysis of Bcr-Abl phosphorylation. Leuk Res (2011), doi:10.1016/j.leukres.2011.01.012

6 months after the induction of imatinib, and resistance means failure to achieve such a response. On the other hand, in nilotinib- or dasatinib-treated patients, a "response" means a minor cytogenetic response (mCyR) at 3 months or partial cytogenetic response (PCyR) at 6 months after the induction of the second generation TKI, and resistance means failure to achieve this response.

Ten microliters of the PB samples were obtained from patients with informed consent at the beginning or before the initiation of imatinib, nilotinib or dasatinib. Half of each sample was used for examination of the Bcr-Abl sequence, which was performed by the SRL Co. (Tokyo, Japan), and the other half was used for immunoblot analysis.

Approvals for the study were obtained from the institutional review boards of all the participating facilities.

2.2. Reagents

Imatinib, methanesulfonate salt was kindly provided by Novartis Pharmaceuticals (Basel, Switzerland), and nilotinib and dasatinib were purchased from LC laboratories (Boston, MA). The antibodies used in this study were as follows: anti-Lyn, anti-phospho-Crkl, anti-phospho-c-Abl from Cell Signaling Technology (Beverly, MA), anti-phospho-Lyn(Y396) from Epitomics (Burlingame, CA), anti-Crkl, anti-β-actin from Santa Cruz Biotechnology (Santa Cruz, CA), and the secondary antibodies, anti-Rabbit IgG HRP and anti-Goat IgG HRP were from Promega (Madison, WI). Pervanadate was purchased from Sigma–Aldrich (St. Louis, MO).

2.3. Cell line

A Bcr-Abl positive human cell line, K562, was used in the preliminary experiments in this study. K562 cells were maintained in RPMI1640 (nacalai tesque, Kyoto, Japan) supplemented with 10% fetus bovine serum (FBS) (EQUITECH-BIO, Kerrville, TX).

2.4. Immunoblot assays of patients' samples

Whole blood cell samples from patients were used within 3 h after blood had been drawn. Red cells were lysed with Whole Blood Lysing Reagents (Beckman Coulter, Brea, CA), and white blood cells were cultured with or without imatinib, nilotinib or dasatinib. After 5-h incubation, the cell lysates were collected and subjected to immunoblot assays. Gel electrophoresis and immunoblot assays were performed according to methods described previously [17,18]. Immunoreactive proteins were visualized with an enhanced chemiluminescence detection system (PerkinElmer Life Sciences, Boston, MA).

2.5. Evaluation of phosphorylation intensity and determination of the "residual index (RI)"

The intensity of each blot of immunoreactive protein was quantified using ChemiDoc XRS+ with Image Lab Software (Bio Rad, Tokyo Japan). The RI values of each patient to TKIs were determined in accordance with the numerical expression, as indicated in Fig. 2A.

2.6. Statistical analysis

Analysis of variance was used to assess data reproducibility. The Mann–Whitney rank sum was used to define differences between groups.

3. Results

3.1. Immunoblot analysis of phosphorylated Crkl in CML patients

To assess the drug response of the CML patients, we performed immunoblot assays detecting phosphorylated Crkl, a direct target of Bcr-Abl kinase. To establish the experimental procedures, preliminary experiments were performed with K562, a CML blast crisis cell line, or blood sample from a newly diagnosed CML patient (Patient A), 98% of whose PB cells were Bcr-Abl-positive on fluorescence *in situ* hybridization (FISH). First, to determine the optimum incubation period for the TKIs, PB cells were incubated with or without TKIs for varying time periods. A two-hour incubation was not sufficient because imatinib did not completely suppress the phosphorylation of Crkl, while 24-h incubation was too long because the PB neutrophils appeared to die (Fig. 1A, left panel). A five-hour incubation completely eliminated the phosphorylation of Crkl without cell death. On the other hand, simultaneous treatment with a phosphatase inhibitor sustained the phosphorylation of Crkl even after treatment for 24 h (Fig. 1A, right panel). Thus, we decided to incubate cells for 5 h without phosphatase inhibitors. Next, to build an *in vitro* simulation model for the estimation of the activities of TKIs in the body, we fixed the concentrations of TKIs at the peak value of plasma concentrations in patients (Cmax) after administration of the recommended dose of TKIs. The Cmax of imatinib in CML patients after taking orally 400 mg of the drug is 3.0–4.8 μM, and that of nilotinib after taking 400 mg is 2.9–4.0 μM. In the case of

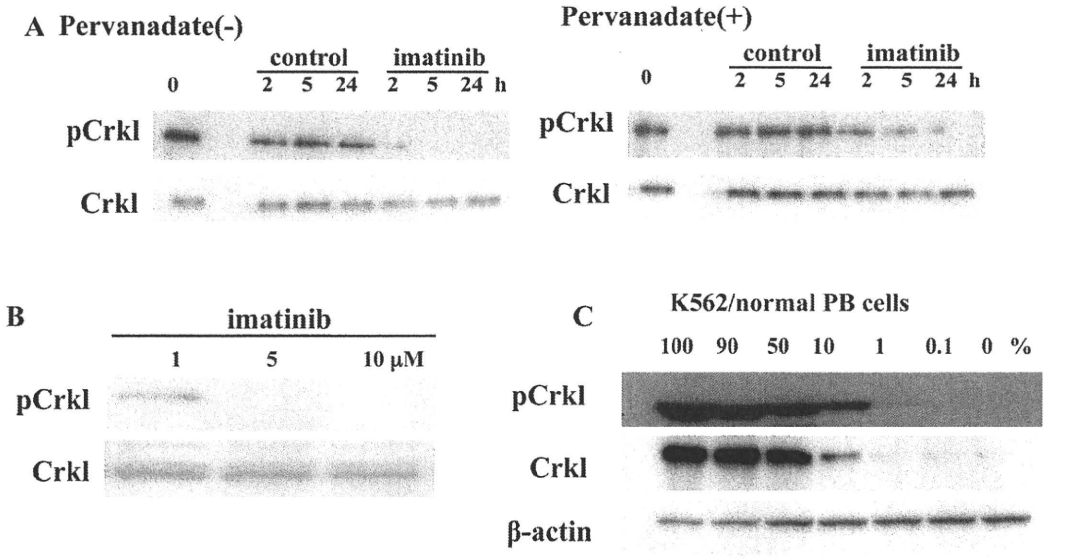

Fig. 1. Optimization of western blot after TKI-incubation. (A and B) Blood sample from Patient A was incubated with or without 5 μM imatinib supplemented with (right panel) or without (left panel) 10 μM of pervanadate for the indicated periods (A) or incubated with imatinib at the indicated concentrations for 5 h (B). The treated cells were lysed and subjective to immunoblot analysis using the indicated antibodies. (C) K562 cells were mixed into normal human PB cells at the indicated ratios. Then the samples were subjective to immunoblot analysis.

Please cite this article in press as: Shibata M, et al. Predictability of the response to tyrosine kinase inhibitors via *in vitro* analysis of Bcr-Abl phosphorylation. Leuk Res (2011), doi:10.1016/j.leukres.2011.01.012

dasatinib, the Cmax after the ingestion of 100 mg dasatinib was 100nM [19–21]. In terms of pharmacokinetics, we fixed the concentrations of these TKIs (imatinib, nilotinib and dasatinib) at 5 μM, 5 μM, and 0.1 μM, respectively. As shown in Fig. 1B, 1 μM of imatinib did not eliminate the phosphorylation of Crkl in the examined sample of patient A who are newly diagnosed and well responded to imatinib, but 5 μM and 10 μM of imatinib did, indicating that 1 μM is too low concentration for estimation of clinical outcome. Finally, to estimate the sensitivity of this system, K562 cells were mixed with normal PB cells at variable ratios, as indicated. Fig. 1C shows that the phosphorylated Crkl at the lowest 1% was detectable in K562 cells. Thus, we analyzed patients having more than 10% Bcr-Abl-positive cells in PB by FISH.

3.2. Iimmunoblot analysis

To quantify the *in vitro* responsiveness to TKIs, we measured the density of each blot using a densitometric method. We then defined "residual index (RI)" for each TKI by the numerical expression as shown in Fig. 2A. Triplicate measurements were performed on 3 individual patients (Patient B, C and D). There were no significant variations among the RIs in each patient. Standard error for each sample set was less than 5% (4.6%, 1.2% and 3.4%, respectively) (Fig. 2B).

3.3. Responses to the TKIs in patients with various stages of CML

Fig. 3A represents typical results of the immunoblot analyses in 2 patients with newly diagnosed CML (Patient 1 and 2), and 2 patients who were receiving imatinib but were displaying resistance (Patient 16 and 17). Although all of these samples exhibited apparent phosphorylation of Crkl without TKIs, the phosphorylated Crkl disappeared from the samples of Patients 1 and 2 when incubated with imatinib, nilotinib or dasatinib. In the case of Patients 16 and 17, on the other hand, weak bands remained in the imatinib and/or nilotinib-incubated samples, but disappeared in the dasatinib-treated ones. Thus, this immunoblot analysis appeared to be useful in evaluating Crkl phosphorylation after *in vitro* TKI-incubation. All patients were divided into two groups: one being newly diagnosed and another receiving imatinib-therapy but showing resistance. The imatinib-RIs of the samples from the imatinib-resistant group (median RI: 34.2%) were much higher than those of the samples from newly diagnosed patients (median RI: 4.2%) (Fig. 3B).

3.4. Sequential examinations using the residual index

RI values were analyzed sequentially in the course of the different TKI-treatments in 2 imatinib-resistant patients (Patient 23 and 27).

Patient 23 (Fig. 4A): after six months of treatment with imatinib, the drug was changed to dasatinib because of a failure to achieve an optimal response (72% $Ph1^+$ in FISH). Six months after the start of dasatinib, $Ph1^+$ cells were disappeared. The samples were obtained twice: prior to the treatment with imatinib, and at the time of change to dasatinib. Immunoblot analysis showed that neither imatinib nor nilotinib eliminated the phosphorylation of Crkl at the initiation of treatment, but dasatinib did. Furthermore the RI values were under 10% only in the sample incubated with dasatinib.

Patient 27 (Fig. 4B): when the first sample was obtained, the percentage of $Ph1^+$ cells was 93% after 7-year treatment with imatinib.

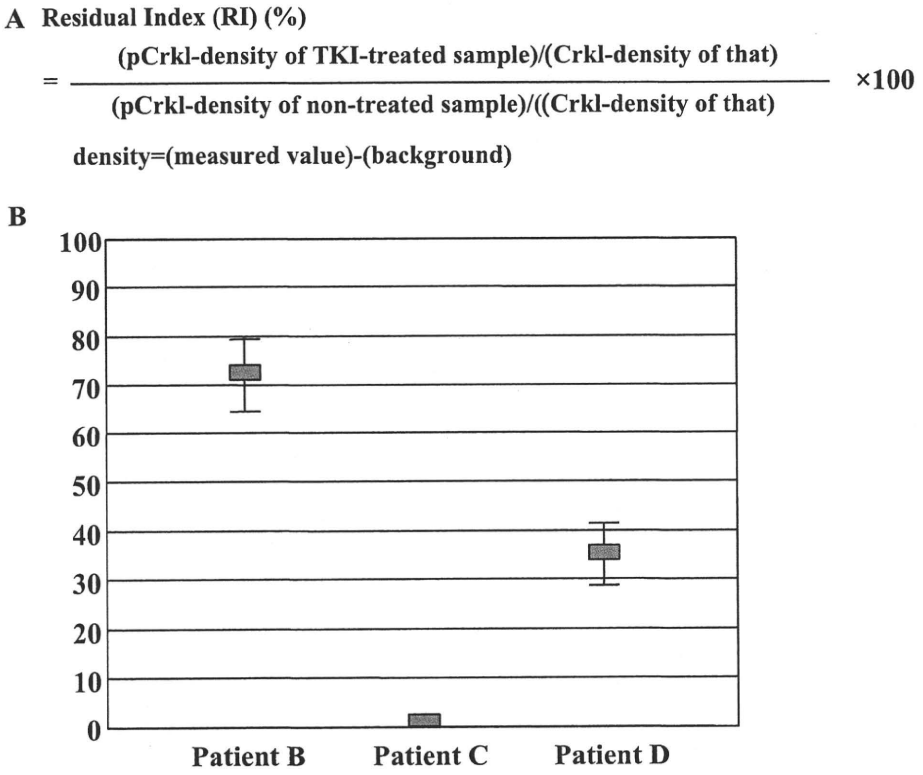

Fig. 2. "Residual index (RI)". (A) The numerical expression of RI. "Measured value" means the density of each blot measured by densitometric method. (B) The reproducibility of RIs for imatinib treatment. Means and standard errors, representing triplicate assays in 3 patients, are shown.

Please cite this article in press as: Shibata M, et al. Predictability of the response to tyrosine kinase inhibitors via *in vitro* analysis of Bcr-Abl phosphorylation. Leuk Res (2011), doi:10.1016/j.leukres.2011.01.012

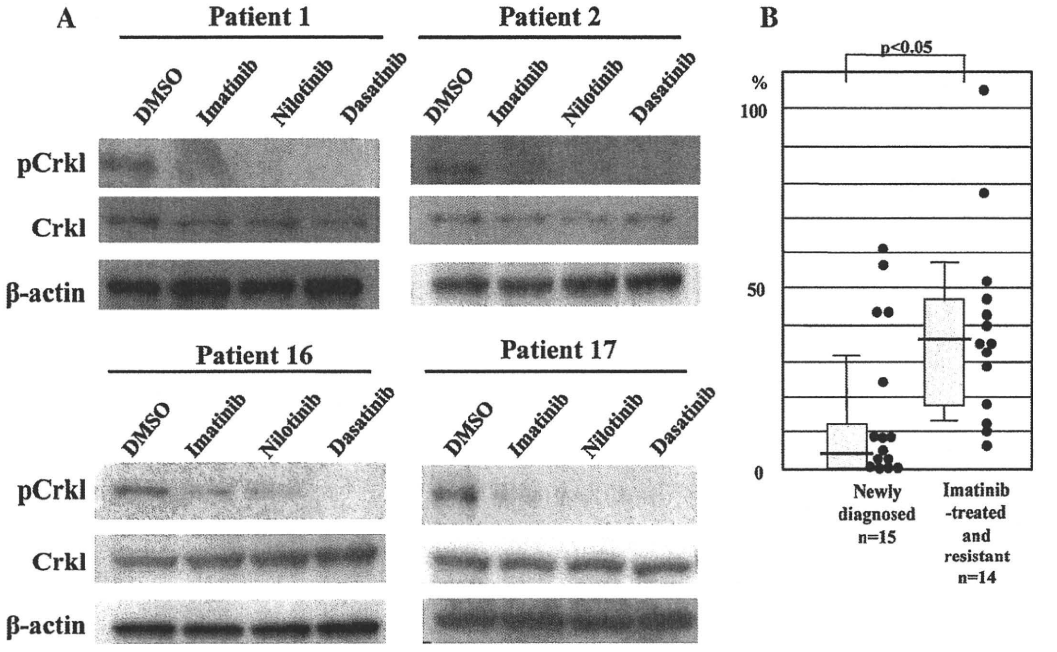

Fig. 3. Different RI values against imatinib between patients at diagnosis and patients showing imatinib-resistance. (A) Four typical data of immunoblots were represented. PB cells from newly diagnosed patients (Patient 1 and 2) or patients (Patient 16 and 17) who had been receiving imatinib-therapy but showed its resistance were incubated for 5 h *in vitro* with or without indicated TKIs. The concentration of imatinib, nilotinib, and dasatinib are 5 μM, 5 μM, and 0.1 μM, respectively. The incubated cells were lysed and subjected to immunoblot analysis using the indicated antibodies. (B) RIs against imatinib were calculated in 15 patients at diagnosis and 14 patients who had been receiving imatinib-therapy and showed its resistance. The distribution of RIs in each group was plotted. Representative box plots show values within the 25th to 75th percentile. Medians are indicated in crossbar. Fifth and 95th percentiles are shown by error bars. The statistical difference was $p < 0.05$.

Then the treatment was changed to dasatinib, which was stopped because of a strong pancytopenia. The patient was then treated with nilotinib, but the percentage of $Ph1^+$ cells again increased. The second sample was obtained at the time of the change from dasatinib to nilotinib. In both samples, the incubation with the three TKIs did not eliminate the phosphorylation of Crkl. Although the second sample exhibited a strong sensitivity only to dasatinib (RI = 4.1%), the remaining CML cells additionally displayed continuous Lyn-phosphorylation (Fig. 4B).

3.5. RIs in patients with Bcr-Abl point mutations

The most important issue in TKIs resistance is the acquisition of point mutations in Bcr-Abl. Bcr-Abl mutations were detected in 4 samples (Table 2). The RI values of Patient 28, with a threonine-to-isoleucine mutation at codon 315 (T315I), were higher than 10% in all the TKI-treated samples. In accordance with the *in vitro* results, the disease was refractory to both imatinib and dasatinib. A phenylalanine-to-leucine mutation at codon 317 (F317L) and a methionine-to-threonine at codon 351 (M351T) were detected in Patient 27. F317L is reported to confer high responsiveness to nilotinib, while M351T does the same to dasatinib. The RI values of this patient were over 10% in all of the samples treated with TKIs, which conformed the outcome of failing to achieve CHR after nilotinib or dasatinib treatment. Next, the RI value in the sample with the phenylalanine-to-valine mutation at codon 359 (F359V) (Patient 23) was less than 10% only in the dasatinib-treated sample, which does not conflict with the reported IC50 data. Finally, although the F317L mutation is reported to be highly sensitive to nilotinib, the RI value for nilotinib in Patient 19, who later proved to be resistant to nilotinib but responded to dasatinib, was higher than 10%, and lower than 10% for dasatinib. Therefore, RIs are likely to be highly correled with the favorability of Bcr-Abl mutations to TKIs, and in some cases, to predict the responsiveness with higher sensitivity than mutations.

3.6. Correlation of RI with patient outcome

To analyze whether the RIs correlate with the clinical response to TKIs, newly diagnosed patients ($n = 15$) were separated into two groups in accordance with the most recent outcome, imatinib-sensitive ($n = 13$), who achieved an optimal response after the sample collection, and imatinib-resistant ($n = 2$), who did not. The median RI of the patients in the sensitive group was 4.2% and that in the resistant group was 43.2% ($p < 0.05$) (Fig. 5, left panel). We also assessed the predictability of the response to nilotinib. Eight patients imatinib resistant had undergone nilotinib-therapy. Among them, 4 achieved optimal responses and the others failed. The median RI in the nilotinib-sensitive group was 3.5% in contrast to 31.2% in the resistant group (Fig. 5, middle panel). Although the sample size was too small to conduct statistical analysis, the RIs were clearly separated between dasatinib-sensitive and -resistant groups (Fig. 5, right panel).

When the cut-off value of RI was set at 10%, the specificities, sensitivities and predicted values were all 100% in terms of nilotinib and dasatinib responsiveness (Table 3). Also, in the evaluation of imatinib-treatment, the specificity and sensitiveness were more than 77%. Therefore, it is suggested that the RIs (cut-off value: 10%) are useful as a novel predictor for clinical utility of TKIs, especially in imatinib-resistant cases.

4. Discussion

Imatinib, the first approved TKI for CML, frequently induces durable cytogenetic remission and thus occupies an important position as the current standard of care. Now, second-generation

Please cite this article in press as: Shibata M, et al. Predictability of the response to tyrosine kinase inhibitors via *in vitro* analysis of Bcr-Abl phosphorylation. Leuk Res (2011), doi:10.1016/j.leukres.2011.01.012

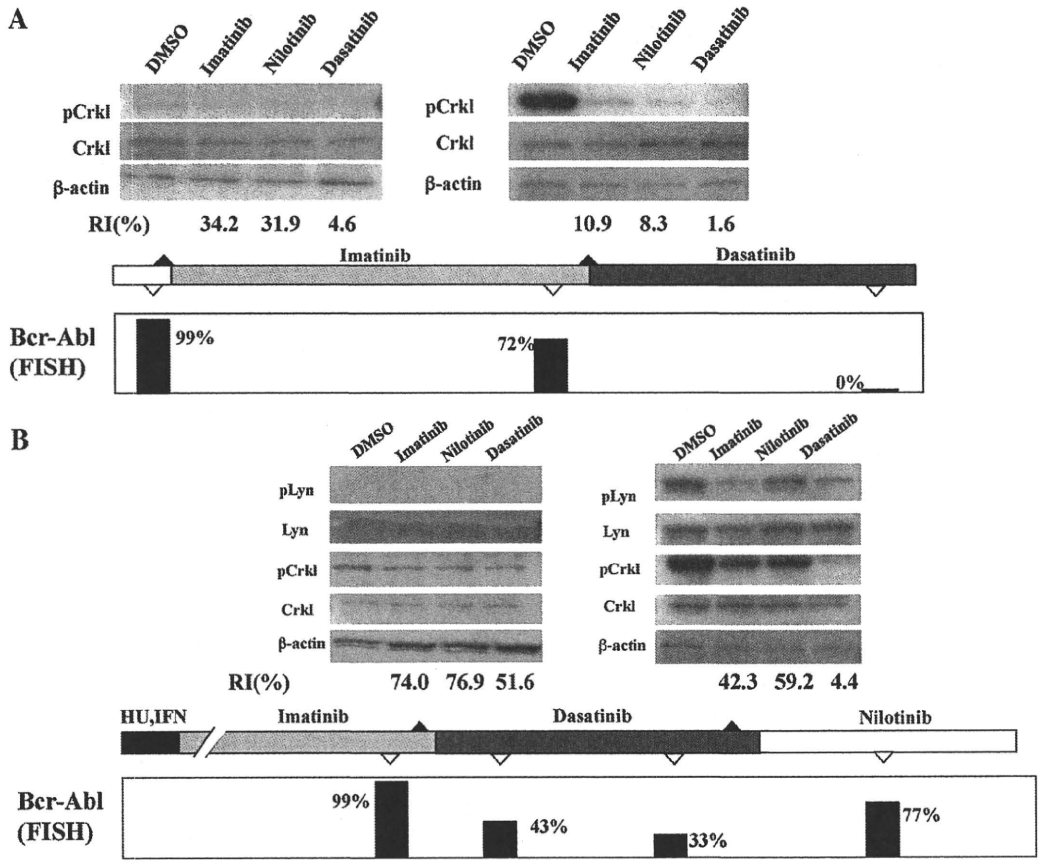

Fig. 4. Sequential examinations of RI values during clinical treatments in two patients. Immunoblots were sequentially analyzed during CML-treatment in two patients who showed resistance to TKIs. Data of immunoblots using the indicated antibodies are shown with their clinical course. FISH analyses are indicated by open triangles, and immunoblot analysis by closed triangles.

Table 1
Patient characteristics.

Characteristic	
No. of patients	31
Median age, y (range)	55 (20–89)
Sex (male/female)	14/17
Treatment before sample collection	
No	13
IFN	3
TKI	18
Bcr-Abl mutation	4
Median follow-up, months (range)	6 (3–14)

TKIs, such as nilotinib and dasatinib, have now been made available [12,13]. Although these TKIs are significantly more potent and show higher sensitivity against some imatinib-resistant mutations, there are no useful guidelines for the proper choice of second-generation TKIs in imatinib-resistant patients. Furthermore, second-generation TKIs have recently been recommended as first-line therapies based on the evidence that an earlier achievement of remission may provide a better clinical outcome or less disease progression. There is still a need for indicators pointing to the proper drug choice for individual patients. The *in vitro* responsiveness to TKIs in terms of cell proliferation has been demonstrated to be a predictor of clinical response. The IC50, a cell based screen for resistance determining the drug concentration that can induce 50% of growth suppression, is a potent predictor of the responsiveness to drugs. In patients with *de novo* CML, the $IC50^{imatinib}$ was reported to possess a high predictive value [22]. However, determination of the IC50 for each TKI requires so much effort and time that an application suitable for all patients may be quite a distant prospect. Furthermore, as the optimal concentration varies for each TKI, comparing the efficacy between different TKIs is difficult. Although the cellular IC50 s for the effect of TKIs on Bcr-Abl point mutations have been reported [23–26], this information

Table 2
Patients with BCR-ABL mutations, and their RI values.

Patient	Mutation	RIs			Clinical outcome
		Imatinib	Nilotinib	Dasatinib	
Patient 19	F317L	40.0	30.8	3.9	Imatinib and nilotinib resistant, and dasatinib respond
Patient 23	F359V	15.8	11.9	1.4	Imatinib resistant, and nilotinib and dasatinib intolerant
Patient 27	M351T/F317L	74.0	76.9	51.6	imatinib resistant, and nilotinib and dasatinib intolerant
Patient 28	T315I	104.2	88.0	93.0	Imatinib and dasatinib resistant

Please cite this article in press as: Shibata M, et al. Predictability of the response to tyrosine kinase inhibitors via *in vitro* analysis of Bcr-Abl phosphorylation. Leuk Res (2011), doi:10.1016/j.leukres.2011.01.012

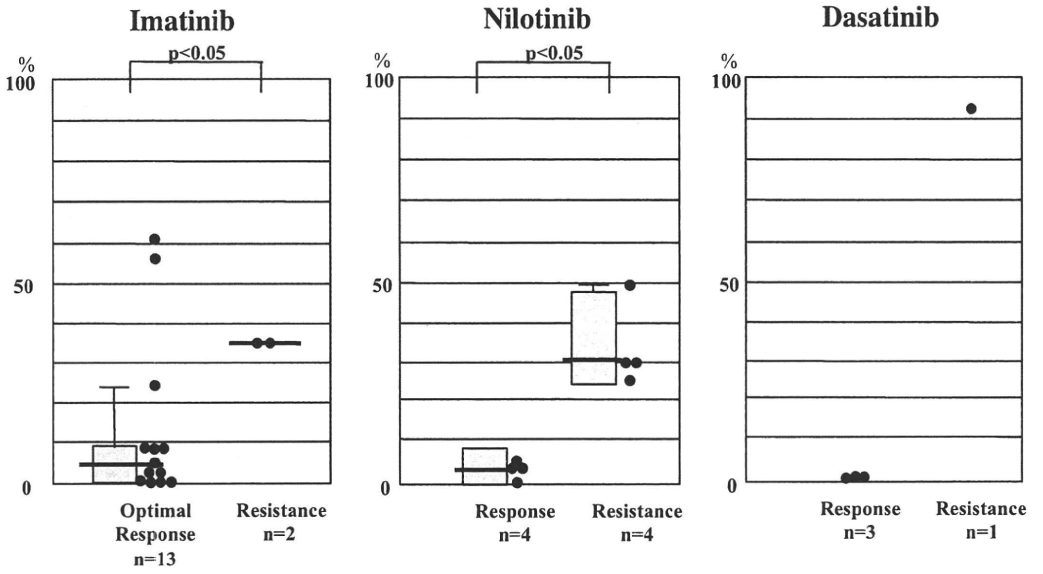

Fig. 5. RI values in patients grouped by clinical response to each TKI-therapy. Fifteen patients were newly diagnosed as CML, and their PB cells were obtained just before the beginning of imatinib-therapy. The patients were divided into two groups: "optimal response" in imatinib-treated patients means *de novo* CML patients who later proved to achieve optimal response, and "Resistance" means patients who later failed to achieve optimal response. Among 12 patients who had showed imatinib-resistance, 8 patients received nilotinib-therapy and 4 patients received dasatinib-therapy at a stretch of imatinib-therapy. Their PB cells were obtained just before the change of therapy. The patients were divided into two groups: that of responsive patients and of resistant patients to each TKI. Dot plots demonstrate the RI values of patients to each TKI. Representative box plots show values within the 25th to 75th percentile. Medians are indicated in crossbar. Fifth and 95th percentiles are shown by error bars.

Table 3
Sensitivity and specificity.

	Optimal response	Resistance	Predicted value
Newly diagnosed and Imatinib-treated patients ($n=15$)			
RI < 10	10	0	100%
RI ≥ 10	3	2	40%
Specificity/sensitivity	77%	100%	
Imatinib-resistant and Nilotinib-treated patient ($n=8$)			
RI<10	4	0	100%
RI ≥ 10	0	4	100%
Specificity/sensitivity	100%	100%	
Imatinib-resistant and Dasatinib-treated patients ($n=4$)			
RI < 10	3	0	100%
RI ≥ 10	0	1	100%
Specificity/sensitivity	100%	100%	
	Newly diagnosed and later achieved optimal response	Imatinib-treated and showed resistance to Imatinib	Predicted value
All included and evaluable patients ($n=27$)			
RI < 10	10	1	91%
RI ≥ 10	3	13	81%
Specificity/sensitivity	77%	93%	

is only useful when the mutated subclone is the predominant cell population.

In this study, we evaluated the effect of TKIs on Crkl phosphorylation as a "residual index". It is noteworthy that the samples from patients who had shown resistance to imatinib had much higher RIs than the samples from newly diagnosed patients. In the case of newly diagnosed patients, most samples responsive to imatinib *in vitro*, but two patients whose samples displayed markedly high RIs *in vitro* proved not to achieve an optimal response to the drug. Although substantial accordance was later detected in the immunoblot data between the responsiveness and resistance to imatinib, a few samples had markedly high RIs in patients who later achieved optimal responses to imatinib. These exceptional cases will have to be followed for a longer period. The data showed 100% of sensitivity and 77% of specificity when the RIs were separated at 10%. On the other hand, in imatinib-resistant patients, the results of the tests did reflect the patient outcome. Although the sample size was small, the immunoblot analysis was able to predict the clinical responsiveness to nilotinib or dasatinib treatment with 100% sensitivity and specificity. Thus, this system can be a useful tool for selecting TKIs, especially in imatinib-resistant patients. It may be inferred that the lower confidence in

Please cite this article in press as: Shibata M, et al. Predictability of the response to tyrosine kinase inhibitors via *in vitro* analysis of Bcr-Abl phosphorylation. Leuk Res (2011), doi:10.1016/j.leukres.2011.01.012